Electronic excitation of the 750- and 811-nm lines of argon

Z. M. Jelenak, Z. B. Velikić, J. V. Božin,* Z. Lj. Petrović, and B. M. Jelenković
Institute of Physics, P.O. Box 57, 11000 Belgrade, Yugoslavia
(Received 11 November 1992)

Measurements have been made on the electron excitation coefficients of four Ar levels: $2p_1$, $2p_5$, $2p_7$, and $2p_9$. Radiative decay of these levels to $1s$ levels is responsible for the strongest line features in argon spectra, at 750 nm due to radiation from $2p_1$ and $2p_5$ levels, and at 811 nm due to transitions from $2p_7$ and $2p_9$ levels. We have measured excitation coefficients of these levels in the range of E/N from 50 Td to 9 kTd (1 Td $=10^{-21}$ V m^2). Here E is the electric field and N is the gas density. The optical emission intensities normalized to the local current density were placed on the absolute scale after normalizing the data for the $2p_1$-$1s_2$ transition (750.4 nm) to the previous experimental and theoretical results at 50 Td. We have also made measurements of the excitation coefficients of several $4d$ and $6s$ vs E/N, in order to estimate the effect of cascading from upper levels to $2p$ levels. We have found that the excitations of $2p_9$ and $2p_7$ are influenced by collisional population transfer between $2p$ levels at low E/N ($E/N < 100$ Td, $N > 2.7\times10^{23}$ m^{-3}), by cascading from $3d$ and $4s$ levels above 100 Td, and by cascading from $4d$ and $6s$ levels at $E/N > 3$ kTd.

PACS number(s): 52.20.Fs, 52.25.Rv, 52.80.Dy, 52.25.Fi

I. INTRODUCTION

Argon atoms play an important role in the kinetics of gas discharges used for excimer lasers [1]. They have also been extensively used for over a decade in plasma processing of various materials [2]. Plasma processing using pure Ar (beam etching) or Ar in the mixtures with reactive gas (reactive etching) are widely used in manufacturing of very-large-scale-integration circuits. In order to optimize the performance of excimer lasers and plasma reactors it is necessary to know the radiative and kinetic processes that occur in argon discharges. Optical emissions from excited states were used to determine the radiative lifetimes and collisional deactivation rates [3], and also to get information on the electron energy distribution function and spatial variation of the electric field in gas discharges. The density of reactive atoms that are important for surface processing was often determined by optical actinometry using the optical emission for argon lines [4].

The optical transitions normally used for the optical diagnostics are those originating from the $3p^5 4p$ levels to $3p^5 4s$ levels. In the Paschen notation which will be used throughout the text the upper and lower states are $2p_n$ and $1s_n$, respectively. Spectral scans of argon discharges show that the strongest features for wavelengths between 250 and 850 nm are emissions at 750 and 811 nm. Each of the features consists of two lines that often are not resolved in the experiments [4,5]. At 750 nm there are transitions between the $2p_1$ to the $1s_2$ level (750.4 nm), and from the $2p_5$ to the $1s_4$ level (751.4 nm). The feature at 811 nm consists of 811.5- and 810.4-nm lines from the transition between the $2p_9$ level to the $1s_5$ level and from the $2p_7$ level to the $1s_4$ level, respectively. Despite the frequent use of these transitions as a diagnostic tool and for testing the different models [5], there are few data on their emission cross sections and rate coefficients. The four levels have different J values and are therefore subject to different rates of population through cascading and population from $1s$ metastable states, something that has to be taken into account in experiments at high gas pressures and currents.

Experimental measurements [6–8] of the excitation cross section of $2p$ levels, including the four involved in the two spectral features at 750 and 811 nm, show a large discrepancy. The results of Chutjian and Cartwright [8] are often used as the set of excitation cross sections for calculations of the rate coefficients for $2p$ levels. The excitation cross sections for the optically allowed $2s$ and forbidden $2p$ levels were calculated by Bretagne *et al.* [9] using Bethe-Born formalism. Their results for $2p$ levels agree well with the measurements of Chutjian and Cartwright [8].

The only measurements of the excitation rate coefficients of $2p$ levels were done by Tachibana using the drift tube [10]. His results cover the range of E/N between 20 and 500 Td. He compared the measured values of the total excitation rate coefficients for all the $2p$ levels with those calculated by Boltzmann analysis, and found good agreement for $E/N > 50$ Td. For his calculations he used the momentum-transfer cross section of Hayashi [11], and the ionization cross section measured by Rapp and Englander-Golden [12]. The cross sections for the total excitation of the allowed and forbidden states (mostly $2p$ state) were taken from Eggarter [13] and corrected for the higher-energy range using the total excitation cross section given by de Heer, Jansen, and van der Kaay [13]. Tachibana considered neither population to $2p$ from upper states, nor the population mixing within the $2p$ multiplet in his experiment, where pressure was between 0.1 and 20 Torr.

The excitation rate coefficients for individual $2p$ levels were also calculated by Puech and Torchin [14] using a two term Boltzmann code. For calculating the electron energy distribution function they used the momentum-

transfer cross section given by Frost and Phelps [15], while for inelastic processes, including the excitation of $2p$ levels, they used the cross sections calculated by Bretagne *et al.* [9]. The set was based on the experimental data of Chutjian and Cartwright. After calculating the excitation coefficients for the upper states that can populate $2p$ levels via cascading, using the set of cross sections from Ref. [9], they found a strong cascade excitation for most of the $2p$ levels. The individual branching rations for the processes corresponding to the cascade population of $2p$ levels from higher levels were calculated using the transition probabilities calculated by Lilly [16]. With the exception of $2p_1$, the population of the other levels studied in this paper seems also to be affected by cascading, specially $2p_9$. No possible effects of radiation imprisonment and collisional mixing of levels are discussed.

In the present work we have measured spatial excitation coefficients of $2p_1$, $2p_5$, $2p_7$, and $2p_9$ levels and, from there, of the 750- and 811-nm lines in the range of E/N, from 50 Td to 7 kTd. The relative measurements of the coefficient were put on the absolute scale after normalizing the data at 750.4 nm at 50 Td to the value of the excitation coefficient of the $2p_1$ level measured by Tachibana [10]. This value is in agreement with results calculated by Puech and Torchin [13] at the same E/N. In order to estimate the contributions to the measured excitation coefficients from the cascading transitions from upper levels the measurements of the excitation coefficients for some of the transitions from $4d$ and $6s$ levels to $2p$ levels were also performed. There are no previous measurements of this kind.

We also present data for ionization coefficients obtained from the fit to the spatial scan of optical emission of lines at 750 and 811 nm. The data are compared with the previous measurements and calculations of ionization coefficients in argon using Boltzmann analyses, single beam models [17], and Monte Carlo calculations.

II. EXPERIMENT

The experimental setup has been described in an earlier publication [18]. The drift tube consists of two plane parallel electrodes with a diameter of 79 mm and distance of 16.6 mm. The cathode was made out of stainless steel, while the anode was made from graphite in order to minimize the effect of backscattered electrons from the anode [5]. They were placed into the close fitting quartz cylinder so that the discharge operating on the left-hand side of the Paschen minimum can be confined between the electrodes.

The argon discharge was running at low current to ensure a uniform electric field. The current was below 2 μA for the highest pressure and below 15 μA for the lowest pressure of the experiment. The range of pressure was between 35 and 0.15 Torr. The operating discharge voltage was then independent of current (to our experimental uncertainty), and the discharge was characterized by the Paschen curve, e.g., by the values of discharge voltage versus Nd, where d is the distance between the electrodes. The Paschen curve of our experiment is shown in Fig. 1. Several straight lines of constant E/N are also shown to indicate the voltage and gas density at different E/N. The current was measured using a Keithley electrometer and the voltage was measured using a voltage probe. The discharge was stabilized by the resistor in series with the discharge, the value of the resistor being

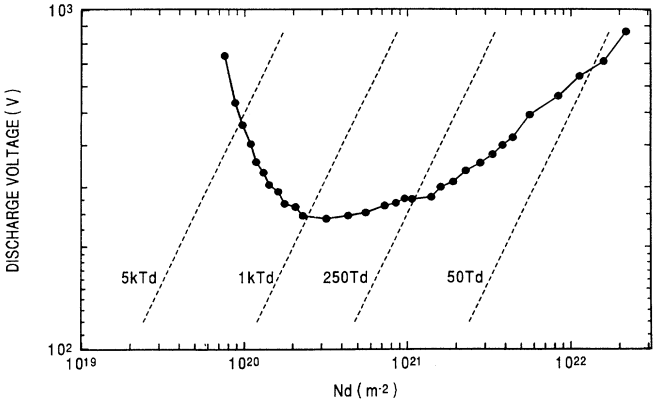

FIG. 1. Discharge voltage vs production of gas density and electrode separation for Ar and for the stainless-steel cathode and graphite anode. The points show our experimental results. The short dashed curves are curves of the constant E/N.

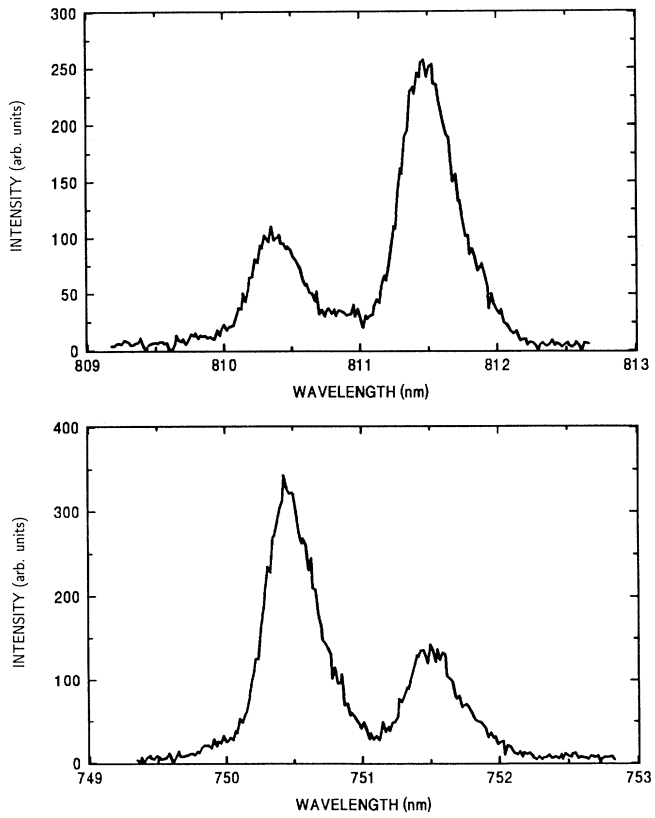

FIG. 2. Argon spectra around 811-nm lines (above) and around 750-nm lines (below) from argon low-current diffuse discharge at 250 Td.

in the range between 1.1 and 4.7 MΩ, for the range of pressure between 0.14 and 35 Torr. The pressure was measured by a mks capacitance manometer. The vacuum in the chamber before the addition of the gas was 10^{-7} Torr, and the rate of rise of background pressure in the chamber was 2 mTorr/h. The argon purity was 99.999%.

The detection of the optical emission was done with a photomultiplier and photon counting chain. Prior to detection the light was spatially resolved with the collimator and spectrally resolved using the monochromator. For measurements of the emission intensities versus E/N, the spectral resolution was below 0.5 nm to insure that the lines were spectrally resolved. The argon spectra around 750- and 811-nm lines at 450 Td are shown in Fig. 2. For the measurements of the light intensity of the four transitions the monochromator was placed at the maximum of the line. The spatially dependent light emission was recorded with the spatial resolution of 1 mm. The entire detection system was placed on the platform and moved by the stepper motor, which was controlled by the computer.

III. RESULTS

A. Ionization coefficients

The spatial scans of argon $2p$ lines show an exponential growth of emission with distance as one approaches the anode up to rather high E/N of 9 kTd. These are much higher E/N than what has been recently observed [19] for hydrogen. The absence of exponential growth occurs when excitation by the runaway electrons or by backscattered electrons from the anode or by heavy particles plays a considerable role in comparison with excitation by electrons that reach an equilibrium in the discharge (see discussion in Ref. [17]). In Fig. 3 the spatial scan of the 750.4-nm line at different values of E/N are shown. A fit to the data such as shown in Fig. 3 gave the values of ionization coefficients. The results are shown in Fig. 4 using the open circles. Also shown in Fig. 4 are the previous results from current growth measurements [20]. The calculations of the ionization coefficients by Tachibana, using the two term Boltzmann analysis [10], are shown with the solid line, while the results of the single beam model at high E/N obtained in Ref. [5] are shown by solid circles, connected with the short-dashed curve. Using the particle-in-cell–Monte Carlo (MC) code [21] and the cross sections given in Ref. [22] we have calculated the ionization coefficients at 5 kTd. The results of the calculations are shown in Fig. 4 by a solid square. Our optical measurements of the ionization coefficients are lower than those from the current growth measurements and Boltzmann calculations for $E/N > 100$ Td, but they seem to give results in reasonable agreement with calculations at very high E/N.

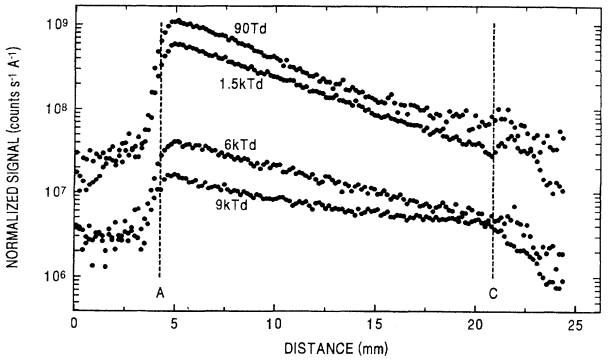

FIG. 3. Normalized emission intensity of the 750.4-nm line, e.g., the transition from $2p_1$ to $1s_2$ at four different E/N. The vertical dashed lines show the positions of the anode (A) and cathode (C).

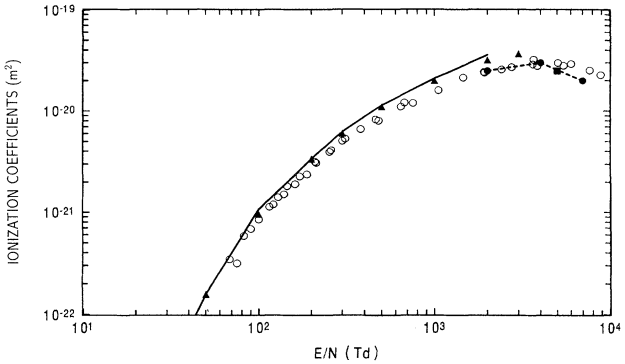

FIG. 4. Spatial ionization coefficients vs E/N. The symbols are as follows: solid triangle, current growth measurements [20]; solid points, results of the single beam model [5]; solid square, PIC-MC calculations; solid line, Boltzmann calculations; open points, present results.

B. Normalization of data

The experimentally observed intensity $S_{mn}(z)$ due to the radiative transition from state m to state n at the distance z from the cathode is related to the spatial excitation coefficient α/N of the state m,

$$\frac{\alpha}{N}=\frac{S_{mn}(z)e}{K_{mn}j_e(z)}(1+N/N_0)\ , \tag{1}$$

where $j_e(z)$ is the current density at the position z. The constant K_{mn} includes several terms, some of which are wavelength dependent,

$$K_{mn}=(\Omega/4)VA_{mn}/A_m\int F(\lambda)Q(\lambda)T(\lambda)d\lambda\ . \tag{2}$$

Here Ω is the effective solid angle subtended by the detector at the axis of the drift tube, and V is the discharge volume from which the detected radiation was emitted. The factor F, Q, and T depended on the wavelength; F is the fractional transmission of quartz tube, windows, and slits; Q is the quantum efficiency of the monochromator, photomultiplier, and counting chain; and T is the fractional transmission of the monochromator. The A_m/A_{mn} is the ratio of the transmission probabilities of state m and that of the transition from level m to level n, e.g., the ratio of the intensity of total radiation emitted

from state m to that emitted via transition mn. The quenching density N_0 is given by $N_0 = A_m / k_q$, where k_q is the rate coefficient for collisional quenching of the state m.

The simple expression for the excitation coefficients as given by Eq. (1) is good only if repopulation of the excited state due to radiative and collisional transfer from other excited states can be neglected. Nevertheless, we will use Eq. (1) to calculate excitation coefficients from the observed optical signal and compare the results with previous data. This in turn will provide us with information as to how important are the cascading and collisional mixing.

The detection system was positioned at $z = 1.1$ mm from the anode. Because the electron current is changing within the distance of the full width at half maximum (FWHM) of the spatial resolution, the electron current density of Eq. (1) was calculated for each E/N from

$$j_e(z) = \frac{1}{\Delta z} \int_{z-\Delta z/2}^{z+\Delta z/2} j_a \exp\left[-\left[\frac{\alpha}{N} \right]^i N z \right] dz \ , \qquad (3)$$

where Δz is equal to the FWHM of the spatial resolution, $j_a = I_a / A$, I_a is the measured discharge current, and A is the anode area. For the ionization coefficient $(\alpha/N)^i$, we recorded our experimental results (Fig. 4) at different E/N.

In another approach for measuring the excitation coefficients we have calculated the anode signal S_a without determining the anode position z_a, using measured spatial dependence of optical emission $S_e(z)$. When the real spatial dependence of the optical emission, given by $S_a \exp[-\alpha(z - z_0)]$ for $z \geq z_a$ and equal to zero for $z < z_a$, was convoluted with the rectangular function of the instrumental spatial resolution, different analytical expressions were then obtained at different positions around the anode, i.e., for $z > z_a + \Delta z$, for $z_a - \Delta z < z < z_a + \Delta$, and for $z < z_a - \Delta z$. Using those expressions to fit the three corresponding parts of the experimental spatial profile $S_e(z)$, we have determined the values of z_a and S_a. The fit to the $S_e(z)$ for $z > z_a$ does show that $S_e(z)$ decreases exponentially from the anode, the α being the ionization coefficient. The calculated anode signal S_a was then normalized to the anode current I_a, and Eq. (1) was used to obtain the excitation coefficients. The latter procedure eliminates the uncertainty in determination of the anode position. The comparison of the results taken from different procedures will be given for the $2p_1$ level.

The values for N_0 for our four levels were obtained from the measured values of the collisional deactivation rate constant and radiative lifetimes for individual $2p$ levels by Chang and Setser [23], Inoue, Setser, and Sadeghi [24], and by Nguyen and Sadeghi [25]. In their work they have done the selective population of one particular argon $2p$ level by laser excitation from the metastable states. From the specific products of different $2p$ levels due to a two-body collision between the laser excited $2p$ level and ground-state argon, they have determined the rate constants for the individual product states. Chang and Setser measured the total destruction rate of the excited states due to collisions of most of the $2p$ levels except $2p_5$ and $2p_1$. Nguyen and Sadeghi measured rate coefficients of collisional population transfer between $2p$ levels, including the $2p_5$ level. The data of the quenching rate coefficients and quenching density used in our data analyses for the four levels are given in Table I.

The values of the factor K_{mn} necessary to obtain the absolute excitation coefficients of the four levels were determined in the following manner. The value for K_{mn} was determined first for two lines at 750 nm by normalizing the signal at 750.4 nm, e.g., $S_{(750.4)} e(1 + N/N_0)/j_e$, to the values of the excitation coefficient of $2p_1$ at 50 Td given by Tachibana [10]. His results at 50 Td are in agreement with calculations by Puech and Torchin [14]. The relative dependence of the quantum efficiency of the detection system between 700 and 840 nm was determined using the spectrum of the $2p$-$1s$ transitions, e.g., the intensities of spectral lines originating from the same upper level and the branching ratios of these transitions. The transition probabilities of different $2p$-$1s$ transitions were taken from Wiese, Smith, and Miles [26]. There is very little difference for the transition probabilities for the $4p$-$4s$ transitions when the data of Ref. [26] are compared with those calculated by Lilly [16].

Except for the 810.4-nm line the other three of the four transitions are the only, or by far the dominant, transitions for radiative destruction of the upper state. The $2p_1$ level decays also to the $1s_4$ level, but via very weak 667.7-nm radiation. Therefore, the ratio A_{mn}/A_m in Eq. (2) for the three states $2p_1$, $2p_5$, and $2p_9$, was set to 1. The level $2p_7$ decays to all four $1s$ levels. The branching ratio $A(2p_7 - 1s_4)/\Sigma A(2p_7 - 1s_n)$ is 0.74 as calculated by Lilly [16], the value that is in good agreement with the results tabulated in Ref. [25]. The value for K_{mn} for the absolute determination of the excitation coefficient for $2p_7$ was corrected accordingly.

C. Excitation coefficients

The results of the excitation coefficient for the $2p_1$ and $2p_5$ levels are shown in Fig. 5. Our measurements are presented by solid triangles, the measurements of Tachibana by open points connected with a dashed line, and the calculations by Puech and Torchin [14] with solid lines. The upper solid line for the excitation coefficients for $2p_5$ was calculated [14] when the cascade excitation

TABLE I. Quenching rate coefficients and radiative lifetimes of $2p$ levels.

Argon levels	k (10^{-17} m^3 sec^{-1})	N_0 (10^{23} m^{-3})
$2p_1$[a]	2.9	16
$2p_5$[b]	2.1	22(9)[c]
$2p_7$[d]	7.7	4.5
$2p_9$[d]	5.9	6

[a]Reference [23].
[b]Reference [24].
[c]From the fit of experiment to the theory [14] at low E/N.
[d]Reference [25].

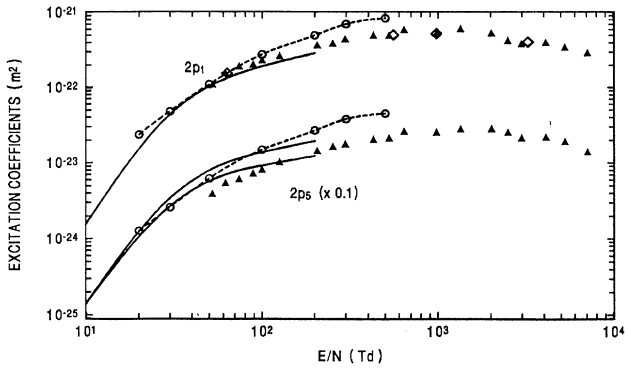

FIG. 5. Spatial excitation coefficients of $2p_1$ and $2p_5$ levels vs E/N. Presented with open points and connected with dashed lines are the results of Tachibana [10]; solid curves are the Boltzmann calculations of Puech and Torchin [14], with the upper one for $2p_5$ including cascading; solid triangles are our results.

was taken into account. For the level $2p_1$ it was found [14] that the direct excitation remains the main production process. Shown with the open diamonds are our results for the excitation coefficient for the $2p_1$ level when the anode signal, determined from the procedure described in Sec. III B, was used instead of the signal at 1.1 mm from the anode. The agreement between the two sets of data is satisfactory. Our results for $2p_1$ are in better agreement with calculations [14] than with the experiment [10]. Comparing our results with Tachibana's results for the $2p_5$ level, we can see the similar E/N behavior but a difference in magnitude of about a factor of 2. At lower E/N our results are considerably lower than calculations [14]. But we have to keep in mind here that for the $2p_5$ level we have used a value of N_0 which includes only the $2p$ intramultiplet quenching [24]. A value of 9.2×10^{23} m^{-3} for the quenching density of the $2p_5$ level will be necessary to get good agreement with calculations [14] between 60 and 120 Td (Table I).

In Figs. 6 and 7 we have shown the excitation

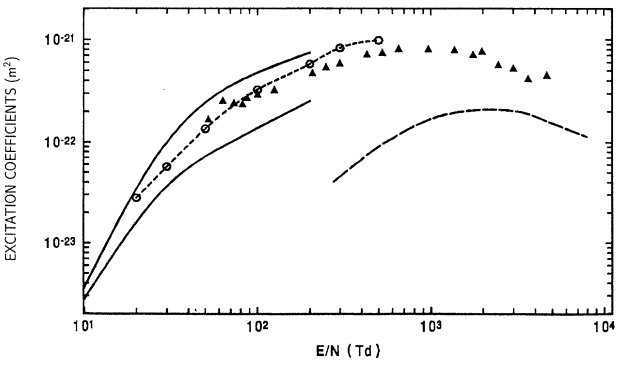

FIG. 6. Spatial excitation coefficients for the $2p_9$ level vs E/N. The long-dashed curve is our estimate of the cascading from $4d$ levels. The other symbols are the same as in Fig. 5.

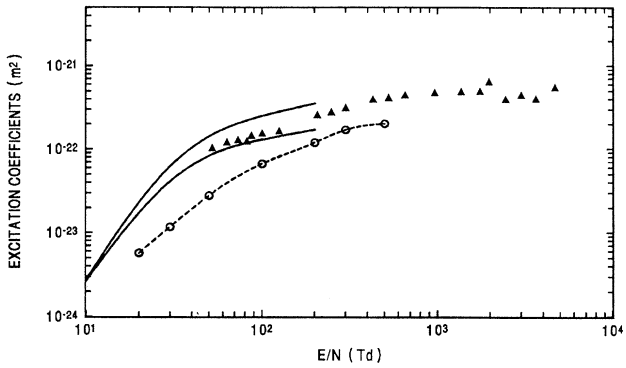

FIG. 7. Spatial excitation coefficients of the $2p_7$ level vs E/N. The symbols are the same as in Figs. 5 and 6.

coefficients for $2p_9$ and $2p_7$ levels, respectively. The difference exists between our data and Tachibana's data both in the magnitude and in the variation with E/N for $2p_7$ level. Our excitation coefficients for both levels fall between the two solid lines representing the calculations of Puech and Torchin [14]. The long dashed curve in Fig. 7 is our estimate of the cascading contribution from the upper $4d$ levels (see discussions in the next section).

Figure 8 shows the excitation coefficients of the two lines, 750 and 811 nm. The solid lines are those calculated by Puech and Torchin [14] when cascading from upper states is not included. Although we disagree with Tachibana on the results of the excitation coefficients for $2p_9$ and $2p_7$, the total excitation coefficients for the 811-nm line presented here and in Ref. [10] are in agreement.

D. Cascading and collisional mixing

The $2p$ levels can be populated via cascading from the upper $3p^5ns$ and $3p^5nd$ levels. We were not able to detect the transition from $3d$ and $5s$ levels to $2p$ levels because these are in the infrared region. We have measured the excitation coefficients for transitions from some $4d$ and $6s$ levels to $2p$ levels for E/N from around 200 Td to 7 kTd. For normalizing the data to the absolute values of the excitation coefficients, the same value for K_{mn} [Eq. (1)] was

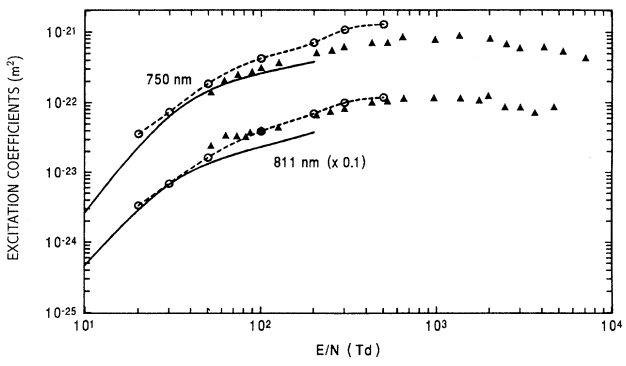

FIG. 8. Total excitation coefficients of the 750- and 811-nm lines vs E/N. The solid curves are for the Boltzmann calculations [14] without cascading.

used as for $2p_1$, since our estimates of the relative values of the quantum efficiency of the detector (see Sec. III B) show no variation between 750 and 650 nm. The data are not corrected for the collisional quenching. The results for the $4d_3$-$2p_{10}$ transition at 675.2 nm are shown in Fig. 9 with the solid points. The solid lines on the figure are fits to the data. The results of the excitation coefficients of few other transitions from $4d$ levels at 550 and 2500 Td are presented in Table II. Variation of the excitation coefficients with E/N of all measured $4d$ levels are similar to the excitation coefficients of the $4d_3$ level. The other transitions from $4d$ levels not shown here are much weaker or are too weak to be detected. Also shown in Fig. 9 are the excitation coefficients of the transition from $6s$ to $2p$ levels, e.g., $3s_3$-$2p_4$ at 703 nm, while the values of the excitation coefficients of the $3s_5$-$2p_9$ transition at two E/N are shown in Table II.

We have used our results for the excitation coefficients of some of $4d$ levels and the ratio of the measured optical excitation cross section [6] for different $4d$-$2p$ transitions to estimate the total cascade contributions from $4d$ levels. For such an estimation we have used the optical cross sections from Ref. [6] rather than excitation coefficients, e.g., the convolution of the cross sections with the distribution function, because the energy dependence and the threshold for different $4d$-$2p$ transitions according to [6] are very similar. The results of the estimated contribution from $4d$ levels to the excitation of the $2p_9$ level via cascading are shown in Fig. 7 with a long-dashed curve. One has to bear in mind that the excitation coefficients for cascades from $4d$ levels depend on the published results of optical excitation cross section by Ballou, Lin, and Fajen [6]. However, their data are in disagreement with our results for the excitation of $4d_4$, which decays only to the $2p_9$ level via the 737.2-nm line, close to the much stronger $2p_3$-$1s_4$ transition. Their data suggest that this should be the strongest line of the $4d$-$2p$ series, contrary to our measurements. Comparison of measured excitation coefficients of $2p_9$ and $2p_7$ and our estimates on the contribution from higher $4d$ levels show that the cascading is strong at very high E/N, above 3 kTd, in accordance with the fact that the optical emission cross sections and therefore excitation coefficients for higher states peak at higher electron energy and E/N. It was not possible to estimate the contributions from $6s$ levels because there are no data on the transition probabilities and emission cross sections from those levels. Since the main contribution to our four levels from $6s$ levels should be a weak transition at 715.8 nm, the overall population from $6s$ levels is much smaller than from $4d$ levels.

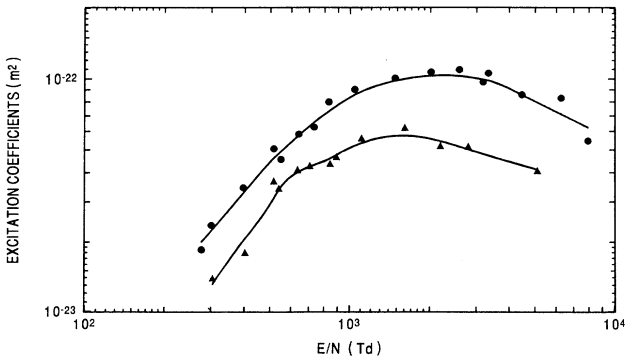

FIG. 9. Excitation coefficients for the transitions from $4d$ and $6s$ levels to $2p$ levels vs E/N. Solid points are the results for the $4d_3$-$2p_{10}$ transition, and solid triangles are the results for the $3s_3$-$2p_4$ transition.

TABLE II. Excitation coefficients of $4d$-$2p$ transitions in units of 10^{-23} m^2.

		α/N (10^{-23} m^2)	
Transition	λ (nm)	550 Td	2500 Td
$4d_3$-$2p_{10}$	675.2	5.0	11.0
$4d_5$-$2p_{10}$	687.1	4.8	9.1
$4d_6$-$2p_{10}$	693.7	2.5	4.8
$4d_4$-$2p_9$	737.2	2.8	
$3s_3$-$2p_4$	715.8	3.3	5.3
$3s_5$-$2p_9$	703.0	2.5	5.7

The effects of cascading from $3d$ levels, as suggested by Puech and Torchin [14], have to be taken into account for all $2p$ levels except $2p_1$. The high gas density at low E/N of our experiment can introduce additional effects on the density of $2p$ states through imprisonment of radiation and collisional repopulation of excitation between $2p$ levels. The allowed transitions to the ground state, subject to imprisonment, arise only from ns and nd levels with $J=1$. Although such levels cannot cascade, for example, to the $2p_9$ ($J=3$) level, density can be influenced via collisional mixing from other $2p$ levels to which a transition from optically allowed levels is possible. On the other hand, for the pressures of our experiment and due to imprisonment, transitions to the $2p_7$ can be the only decaying channel for some optically allowed upper levels [26–28]. In order to estimate the effect of population mixing, cascading, and radiation imprisonment on the density of our four $2p$ levels, we have solved coupled differential equations for the temporal evaluation of their density, with similar equations for the density of upper $3d$ and $5s$ levels. The upper levels include those which are optically allowed, like $3d_2$, $3s'_1$, $2s_2$, and $2s_4$, and those which cannot radiate to the ground state, $3d_{3-6}$, $3d'_4$, and $3s''''_1$. Therefore we have solved simultaneously ten differential equations for $2p$ levels

$$\frac{dN_j}{dt} = k_e^j N n_e + \sum_i k_{q_{i-j}} N_i N - \sum_i k_{q_{j-i}} N_j N - k_{q_j} N_j N - A_j N_j + \sum_k A_{kj} N_k \ , \tag{4}$$

and ten equations for $3d$ and $4s$ levels

$$\frac{dN_k}{dt} = k_e^k N n_e - \sum_j A_{kj} N_k - \nu_k N_k \tag{5}$$

for different E/N, where N is the corresponding density as in the experiment. Here, k_e^x is the rate of electron excitations from the ground state (the data were taken from

Ref. [14]); n_e is the electron density and was calculated for the current of the experiment and using the drift velocity versus E/N from [14]; $k_{q_{ij}}$ is the rate constant for intramultiplet cascade taken from Ref. [24]; k_{qj} is the intermultiplet quenching coefficient leading to formation of $1s$ levels and taken from Ref. [22]; A_j and A_{kj} are transition probabilities for level j and for transition k-j, respectively, and were taken from Refs. [16] and [25]; the summation in the third term in Eq. (5) is over $2p$ levels to which the $3d$ level decays; the third term in Eq. (5) is the transition probability for the decay to the ground state, where ν is the imprisonment decay constant calculated from Holstein's theory [29] and the transition probability of the radiation state for the total radiation imprisonment, using

$$\nu_k = 0.205 A_k \sqrt{\lambda/R} \ , \tag{6}$$

where R is the radius of the discharge cell; and λ is the wavelength of the transition to the ground state. The results of the calculations for the densities of our four levels at 100 Td and 8.6 Torr are shown in Fig. 10. The calculated densities, taking into account both collisional mixing (solid points) and cascading, including radiation imprisonment (solid triangles), were normalized to the density when those processes were neglected. The calculations were performed for E/N up to 200 Td. For general results are that below 100 Td the effect is primarily due to collisional transfer of radiation, while for $E/N > 100$ Td cascading is the major factor. The contribution solely by cascading from $3d$ and $5s$ is similar to the findings in Ref. [14]. This is not surprising since we had used their rate coefficients for excitation for upper levels.

Our results of the effects of collisional mixing and cascading show that the $2p_1$ level is not influenced by either process for $E/N \leq 100$ Td. This in turn supports our calibration procedure when we have normalized emission data to excitation coefficients of $2p_1$ [10,14] at 50 Td. At 200 Td we have found that the cascading and radiation imprisonment can account for up to 15% for the additional population of $2p_1$. The strongest effect is on the $2p_9$ level. Due to collisional mixing at 50 Td and 35 Torr its density is two times in comparison with the case when collisional mixing was not taken into account; due to the cascading and radiation imprisonment at 200 Td and 3 Torr it is nearly a factor of 4 higher.

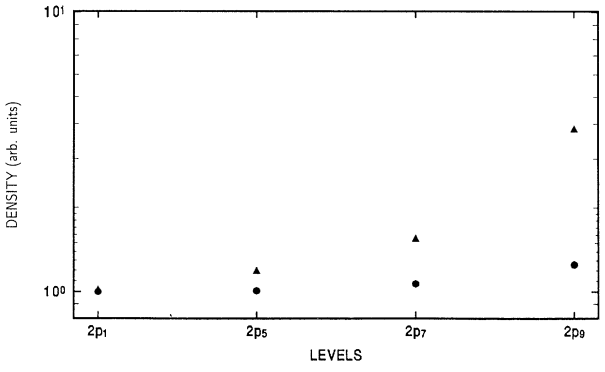

FIG. 10. Density of excited $2p$ levels at 100 Td. The solid points are the results of calculated densities when collisional mixing within the $2p$ levels was taken into account. The corresponding solid triangles are results when both collisional mixing and cascading, with radiation trapping, were taken into account. The results were normalized to the densities calculated when these processes were neglected.

When the results for excitation coefficients of $2p_9$ are corrected for the calculated effect of collisional mixing for $E/N \leq 100$ Td, good agreement was obtained with calculations [14]. But our experimental results around 200 Td show that the cascade contribution can increase the excitation coefficients by a factor of 2, not 4 as obtained from calculations. Our results are reaching the higher level expected from calculation but at $E/N > 500$ Td. We have found similar results for the analyses and comparisons with calculations for the $2p_7$ level.

From the analyses given in this section we have found that Eq. (1) can be used for the excitation coefficients in our experimental conditions only for some $2p$ levels, like $2p_1$, while for the others it at best gives an approximation to the real excitation coefficients. Care must be taken to account for collisional repopulation in the measured light intensity for $E/N < 100$ Td and $N > 3 \times 10^{23}$ m^{-3}, and cascading for higher E/N. Finally, comparing the overall effect of those processes on the two line features 811 and 750 nm, we have found that the intensity of the former is increasing much more due to both collisional mixing and cascading, at both high gas density and high E/N argon discharge.

IV. CONCLUSION

We have presented here the data on the ionization and excitation coefficients of transitions that contribute to two important line features in argon spectra at 750 and 811 nm. The excitation coefficients of $2p_1$ and $2p_5$ levels, which make the line at 750 nm and the excitation coefficients of $2p_7$ and $2p_9$ levels, contributing to the line at 811 nm, were measured in the range of E/N from 50 Td to 7 kTd. The measured light intensity normalized to the current was converted to the excitation coefficients by assuming that the only population mechanism is the electron excitation of the argon in the ground state. Generally there is disagreement between our measurements and those by Tachibana [10] for all four levels. The comparison was also made with the recent calculations by Puech and Torchin [14], who, in addition to the direct electron excitation coefficients of the $2p$ levels, had calculated the excitation coefficients for cascades from the upper levels. Our results for the excitation coefficients for $2p_1$ have shown relatively good agreement with calculations without the contribution from cascading [14] in both magnitude and E/N dependence. For $2p_7$ and $2p_9$ our results fall in between the results from Ref. [14] when cascading was and was not included in the calculations.

From measured excitation coefficients of some $4d$ and $5s$ levels we have found that the cascading from those levels to $2p$ levels can be important only at very high E/N, greater than 3 kT. From calculated contribution to the density of the excited $2p$ levels due to collisional repopu-

lation from other $2p$ levels, and due to cascading from $3d$ and $2s$ levels, and taking the radiation imprisonment into account, we have obtained the results for the above effects on the measured excitation coefficients of $2p$ levels. We have found that none of the processes mentioned above influences the $2p_1$ population; that the biggest effect due to collisional mixing is of the factor of 2 and it is for $2p_9$ at 50 Td and 35 Torr; that the cascading is the most important also for $2p_9$, increasing the population four times at 200 Td; and that the radiation imprisonment has the larger effect on $2p_7$ and is about 10% at 100 Td.

Our experimental results, after being corrected for collisional mixing and cascading, are in good agreement with calculations by Puech and Torchin [14] at $E/N < 120$ Td. Present experiment gives smaller excitation coefficients for $2p_5$, $2p_7$, and $2p_9$ levels at around 200 Td than calculations with cascading, but at $E/N > 500$ Td the results are reaching the level obtained by extrapolating the calculations [14]. Our results also show that the 811-nm line is much more affected by collisional and radiative depopulation at both high density and high E/N argon discharges than the 750-nm line.

ACKNOWLEDGMENTS

We would like to thank to Dr. A. V. Phelps, who had suggested the work. This work was supported in part by the Serbian Ministry of Science and the Yugoslav-USA Fund for Scientific and Technological Cooperation under research Contracts No. 924 and No. 926.

*Also at Faculty of Physics, University of Belgrade, 11 000 Belgrade, Yugoslavia.

[1] *Excimer Lasers,* edited by C. K. Rhodes (Springer Verlag, Berlin, 1979).
[2] H. F. Winters, J. Vac. Sci. Technol. A **63**, 1997 (1988); A. J. van Roosmalen, Vacuum **34**, 429 (1984); U. Gerlach-Meyer, J. W. Coburn, and E. Kay, Surf. Sci. **103**, 177 (1981); D. J. Oostra, A. Haring, and A. E. de Vries, J. Vac. Sci. Technol. B **4**, 1278 (1986).
[3] R. S. F. Chang and D. W. Setser, J. Chem. Phys. **69** (1979).
[4] J. W. Coburn and M. Chen, J. Vac. Sci. Technol. **18**, 353 (1981); S. E. Savas, Appl. Phys. Lett. **48**, 1042 (1986); S. Radovanov, B. Tomčik, Z. Lj. Petrović, and B. M. Jelenković, J. Appl. Phys. **67**, 97 (1990).
[5] A. V. Phelps and B. M. Jelenković, Phys. Rev. A **38**, 2975 (1988).
[6] J. K. Ballou, C. C. Lin, and F. E. Fajen, Phys. Rev. A **8**, 1797 (1973).
[7] I. P. Bogdanova and S. V. Yurgenson, Opt. Spektrosk. **62**, 471 (1987) [Opt. Spectrosc. (USSR) **62**, 281 (1987)].
[8] A. Chutjian and D. C. Cartwright, Phys. Rev. A **23**, 2178 (1981).
[9] J. Bretagne, G. Callede, M. Lengetil, and V. Puech, J. Phys. D **19**, 761 (1986).
[10] K. Tachibana, Phys. Rev. A **34**, 1007 (1986).
[11] M. Hayashi, Institute of Plasma Physics, Nagoya University Report No. IPPJ-AM-19, 1981 (unpublished).
[12] D. Rapp and P. Englander-Golden, J. Chem. Phys. **43**, 1464 (1965).
[13] E. Eggarter, J. Chem. Phys. **62**, 833 (1975); F. J. de Heer, R. H. J. Jansen, and W. van der Kaay, J. Phys. B **12**, 979 (1979).
[14] V. Puech and L. Torchin, J. Phys. D **19**, 2309 (1986).
[15] L. S. Frost and A. V. Phelps, Phys. Rev. A **127**, 1538 (1964).
[16] R. A. Lilly, J. Opt. Soc. Am. **66**, 245 (1976).
[17] A. V. Phelps, B. M. Jelenković, and L. C. Pitchford, Phys. Rev. A **36**, 5327 (1987).
[18] V. Stojanović, J. Božin, Z. Lj. Petrović, and B. M. Jelenković, Phys. Rev. A **42**, 4983 (1991).
[19] Z. Stokić, M. M. Fraga, J. Božin, V. Stojanović, Z. Lj. Petrović, and B. M. Jelenković, Phys. Rev. A **45**, 7463 (1990).
[20] A. A. Kruithof, Physica (Utrecht) **7**, 519 (1940); J. Dutton, J. Chem. Phys. Ref. Data **4**, 577 (1975).
[21] R. Boswell and I. J. Morey, Appl. Phys. Lett. **52**, 21 (1988); C. K. Birdsall, IEEE Trans. Plasma Sci. **19**, 65 (1991).
[22] L. J. Kieffer, JILA Information Center, Boulder, CO, Report No. 7, 1969 (unpublished); *ibid.* Report No. 13, 1973 (unpublished).
[23] R. S. F. Chang and D. W. Setser, J. Chem. Phys. **69**, 3885 (1982).
[24] G. Inoue, D. W. Setser, and N. Sadeghi, J. Chem. Phys. **76**, 977 (1982).
[25] T. D. Nguyen and N. Sadeghi, Phys. Rev. A **18**, 1388 (1978).
[26] W. L. Wiese, M. W. Smith, and B. M. Miles, Atomic Transition Probabilities (U.S. Department of Commerce, Washington, D.C. 1969), Vol. 2.
[27] A. V. Phelps, Phys. Rev. **110**, 1362 (1958); **114**, 1011 (1959).
[28] A. Gallagher (private communication).
[29] T. Holstein, Phys. Rev. **72**, 1212 (1947); **83**, 1159 (1951).